Rock Mechanics and Rock Engineering (2024) 57:2645–2659
https://doi.org/10.1007/s00603-023-03712-6

ORIGINAL PAPER

Water Effects on Elastic S-Wave Propagation and Attenuation Across Single Clay-Rich Rock Fractures: Insights from Ultrasonic Measurements

Hui Yang[1] · Huan-Feng Duan[1] · Jianbo Zhu[2] · Qi Zhao[1]

Received: 24 July 2023 / Accepted: 3 December 2023 / Published online: 7 January 2024

Abstract

Though previous studies have shown that the presence of water strongly influences wave responses of rock fractures, water effects on wave behaviours across clay-rich rock fractures have been ambiguous until now. In the present study, we conducted considerable ultrasonic measurements on single rock fractures filled with kaolinite-dominant gouges at varying water saturation degrees to investigate the water effects on elastic S-wave propagation and attenuation across clay-rich rock fractures. The experimental results reveal that the S-wave velocity across single clay-rich rock fractures slightly increases and decreases with the progressively increasing water saturation degree. An increase in water saturation leads to a concave trend of the spectral amplitudes, while it moderately affects the central frequency of transmitted S-waves. In addition, the seismic quality factor across single clay-rich rock fractures follows an exponential growth trend with the water saturation, suggesting the exponentially negative relation between S-wave attenuation and the water saturation. We attribute the water saturation-dependent S-wave attributes across single clay-rich rock fractures to the combined effects of the local flow and the degradation of grain contacts. Compared to P-wave, S-wave exhibits less sensitivity to varying water saturation of clay-rich rock fracture. Upon increasing water saturation, S-waves display similar velocity and central frequency trends with P-waves. The tendencies of spectral amplitude and seismic quality factor for S-waves are approximately opposite to those for P-waves as the water saturation degree increases. We interpret these discrepancies by the fact that S-wave attributes across single water-saturated clay-rich rock fractures mainly depend on the properties of the skeletal frame, while the characteristics of the particles, pore fluid, and skeleton frame dominate P-wave behaviours. The outcomes of the current work facilitate our understanding of the fluid effects on the interaction of waves with clay-rich rock discontinuities.

Highlights

- S-wave velocity and peak spectral amplitude across single clay-rich rock fractures exhibit concave trends upon rising water saturation.
- The increased water saturation modestly affects the central frequency of S-wave propagating across single clay-rich rock fractures.
- The seismic quality factor for S-waves exponentially grows with the water saturation degree of clay-rich rock fractures.
- The higher the S-wave frequency, the higher the wave velocity, the less the wave energy transmission, and the more the wave dissipation.

✉ Huan-Feng Duan
hf.duan@polyu.edu.hk

Jianbo Zhu
jianbo.zhu@szu.edu.cn

[1] Department of Civil and Environmental Engineering, The Hong Kong Polytechnic University, Hong Kong SAR, China

[2] Guangdong Provincial Key Laboratory of Deep Earth Sciences and Geothermal Energy Exploitation and Utilization, Institute of Deep Earth Sciences and Green Energy, College of Civil and Transportation Engineering, Shenzhen University, Shenzhen, China

- The water-induced evolution of peak spectral amplitude and seismic quality factor for S-waves is roughly opposite to that for P-waves.

Keywords S-wave velocity and attenuation · Clay-rich rock fracture · Water effect · Ultrasonic measurement

1 Introduction

Clay minerals are prevalent in rock fractures at different scales and significantly influence the porosity, permeability, sliding stability, and seismic responses of rock masses (Wealthall et al. 2001; Crawford et al. 2008; Ikari et al. 2009; Carpenter et al. 2011; Indraratna et al. 2014; Ba et al. 2016). Understanding seismic wave propagation across clay-rich rock fractures is of great practical and scientific importance for the applications of acoustic waves in many fields of geotechnical engineering and earth sciences, such as safety estimation of infrastructures, resource recovery and production, and seismic hazard analysis (Niu et al. 2008; Hobiger et al. 2012; Jeppson & Tobin 2015).

Many experimental investigations have been conducted to study elastic wave propagation and attenuation across clay-rich rock fractures over the past decades. The ultrasonic measurements performed by Suarez-Rivera et al. (1991) showed that increasing content of the polar liquids (i.e., brine and ethyl alcohol) enhanced S-wave transmission and reduced S-wave reflection, while the varying saturation of the nonpolar liquid (i.e., decane) had no detrimental influence on S-wave responses of the thin montmorillonite clay layer. The quasi-static resonant column test results reported by Fratta and Santamarina (2002) and Cha et al. (2009) revealed that the filling kaolinite clay plays a more prominent role in decreasing S-wave velocity and enhancing S-wave attenuation, while it has a modest influence on P-wave behaviours across filled rock fractures under uniaxial compression. Knuth et al. (2013) conducted ultrasonic tests on synthetic filled fractures subjected to coupled shear deformation and normal loading/unloading cycles. It was found that the artificial fractures filled with pure smectite clay and smectite-quartz mixture exhibited similar trends in wave properties (Knuth et al. 2013). They also observed that wave properties across rock fractures filled with pure quartz significantly change, while those across clay-rich rock fractures display moderate variations during shear-compression load cycles (Knuth et al. 2013). Their work was recently extended by Kenigsberg et al. (2019, 2020) to inspect further the effects of the composition, shear fabric development, and porosity loss of infilling gouges on elastic wave signatures during fracture sliding. The experimental data uncovered that, with increasing smectite clay content, the fabric development gradually reduced the stiffness of the filling gouge layer, overpowering the influences of the shear-enhanced compaction and porosity loss and thus governing the wave properties across gouge-filled fractures (Kenigsberg et al. 2019, 2020).

Though it has been recognized that fluids significantly influence wave behaviours across rock fractures, fluid effects on wave propagation and attenuation across clay-rich rock fractures have not been thoroughly understood (Li and Ma 2009; Suarez-Rivera et al. 1991; Wu and Zhao 2015). The fluid saturation of rock fractures frequently changes with natural and human-made activities such as rainfalls, groundwater flow, fluid injection, and water-based drilling (Anderson et al. 2010). Therefore, the knowledge concerning fluid effects on wave responses of rock fractures is crucial for earth sciences and geotechnical engineering (Mitchell and Soga 2005). In this context, we have conducted extensive ultrasonic tests on single rock fractures filled with water-saturated clay-dominant gouges to determine elastic P-wave signatures across clay-rich rock fractures under varying water saturation (Yang et al. 2023). It has been found that the infillings' mineralogical composition and water saturation have interconnected influences on P-wave behaviours across individual clay-rich rock fractures.

The present study extends our preliminary work to elucidate water effects on S-wave propagation and attenuation across single clay-rich rock fractures. We perform massive ultrasonic measurements on single synthetic rock fractures filled with kaolinite-dominant gouges over a broad water saturation range. Three pairs of ultrasonic S-wave transducers with different default central frequencies (i.e., 0.25 MHz, 0.5 MHz, and 1 MHz) are employed to examine the influences of wave frequency on S-wave behaviours across single clay-rich rock fractures. The experimental results demonstrate the water saturation dependence of S-wave attributes (i.e., wave velocity, frequency spectra, and seismic quality factor) across single clay-rich rock fractures. The possible physical mechanisms for water effects on S-wave responses of single clay-rich rock fractures are discussed based on the water-clay physicochemical interaction, the heterogeneity of fluid saturation, and the local flow effect. Additionally, the discrepancies between the saturation-dependent S- and P-wave attributes are illuminated regarding wave velocity, frequency contents, and seismic quality factor comparisons. The findings of this study could enhance our understanding

of water effects on S-wave behaviours across clay-rich rock fractures and add insights for interpreting seismic data collected from field monitoring.

2 Materials and Methods

2.1 Specimen Preparation

In this study, gabbro rock from Shanxi, China, was chosen to prepare the rock specimens because it has good homogeneity, minor porosity, and high uniaxial compressive strength. The uniaxial compression tests on standard gabbro rock samples under the quasi-static condition with a strain rate of 1×10^{-5} s^{-1} showed that Young's modulus, Poisson's ratio, and uniaxial compressive strength of gabbro rock are 100.36 GPa, 0.29 and 312.44 MPa, respectively (Yang et al. 2023). In addition, laboratory measurements revealed that the gabbro rock has a bulk density of 2818.32 kg/m^3 and a porosity of 0.23%.

We used the kaolinite-dominant clayey soil from Southwest England of the United Kingdom to prepare the filling clay-rich gouge specimens for this study because kaolinite is one of the most abundant clay minerals in natural rock fractures (Crawford et al. 2008). The clayey soil is composed of pure kaolinite (94%), mica (4%), montmorillonite (1%), and feldspar and quartz (1%). The clay-rich gouges obtained by thoroughly mixing the oven-dried clayey soil at a constant weight with varying proportions of distilled water were hermetically rested for 48 h to generate the infilling specimens at different water saturation degrees. The basic properties of those well-prepared wet clay-rich gouge specimens are summarized in Table 1. These clay-rich gouge specimens' shear moduli and viscosities were

Table 1 Basic properties of the prepared clay-rich gouge samples

No. of the kaolinite-rich gouge samples	Degree of saturation S_r (%)	Bulk density ρ (Mg/m^3)	Dynamic viscosity η (kPa s)	Shear modulus G (kPa)
CG-1	48	1.892	1731.07	2620.36
CG-2	56	1.811	850.13	1581.78
CG-3	64	1.774	487.44	767.89
CG-4	72	1.726	282.22	462.16
CG-5	80	1.690	158.28	258.90
CG-6	88	1.662	74.54	143.22
CG-7	96	1.633	37.20	73.04

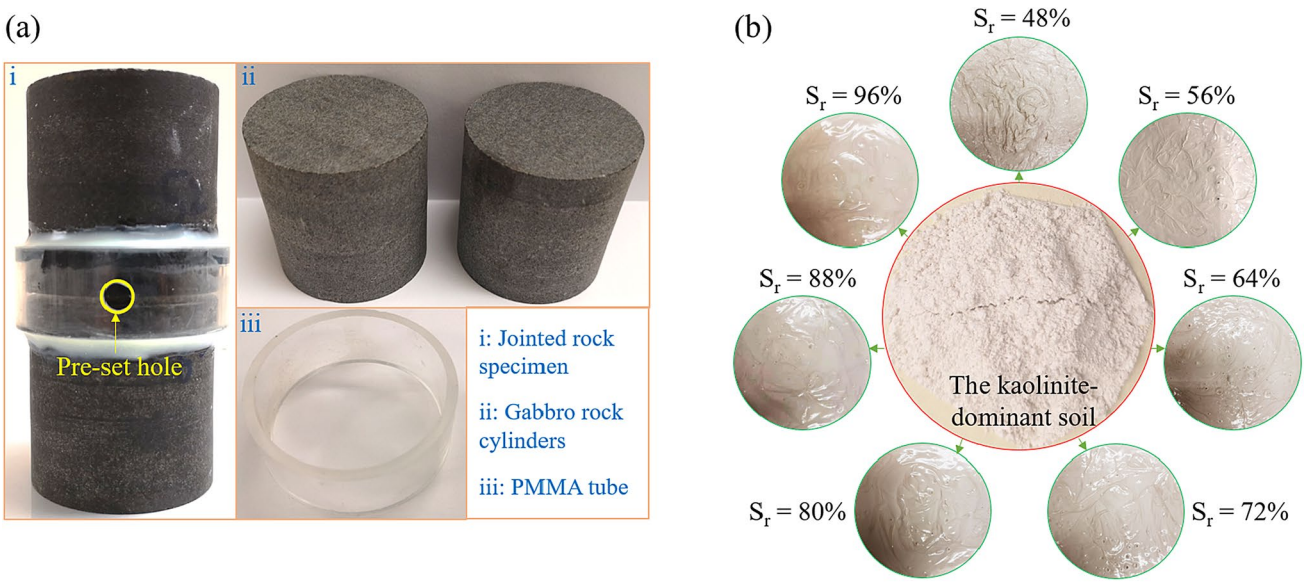

Fig. 1 Materials used for this study: **a** gabbro rock specimens and **b** kaolinite-dominant gouge specimens. S_r denotes the degree of water saturation

measured via a Modular Compact Rheometer using the amplitude sweep method in the low strain range (Mezger 2006). More detailed information on these amplitude sweep tests can be found in Yang (2021).

Herein, an open rock fracture was first generated by combining two gabbro rock cylinders in series via a PMMA tube and epoxy adhesive (Fig. 1a). Both gabbro rock cylinders were about 49 mm in diameter and 49 mm in length. The spacing between these two rock cylinders, i.e., the fracture thickness, was preset as 2 mm. The well-prepared clay-rich gouge specimens (Fig. 1b) were filled into the synthetic fracture separately to create a group of clay-rich rock fractures under various saturating conditions. We also prepared an intact rock sample and an aluminum sample with the same dimensional size as the fractured rock specimen to ascertain reference S-waves.

2.2 Experimental Apparatuses and Procedure

We adopted a self-established ultrasonic test system to carry out ultrasonic measurements on the well-prepared rock specimens for this study. The test system consists mainly of a Tektronix digital oscilloscope (model DPO 2012B), an Olympus Pulser/Receiver (model 5077PR), an ultrasonic S-wave transducer pair, a steel supporting frame, a hydraulic pump, a hydraulic jack, and a personal computer equipped with exclusive software (Fig. 2) (Yang et al. 2020, 2021). Furthermore, three pairs of S-wave transducers with different default central frequencies (i.e., Olympus model V150, V151, and V152) were utilized in this experiment to determine the role of wave frequency in S-wave behaviours across individual water-saturated clay-rich rock fractures. The basic information about those three transducer pairs is given in Table 2.

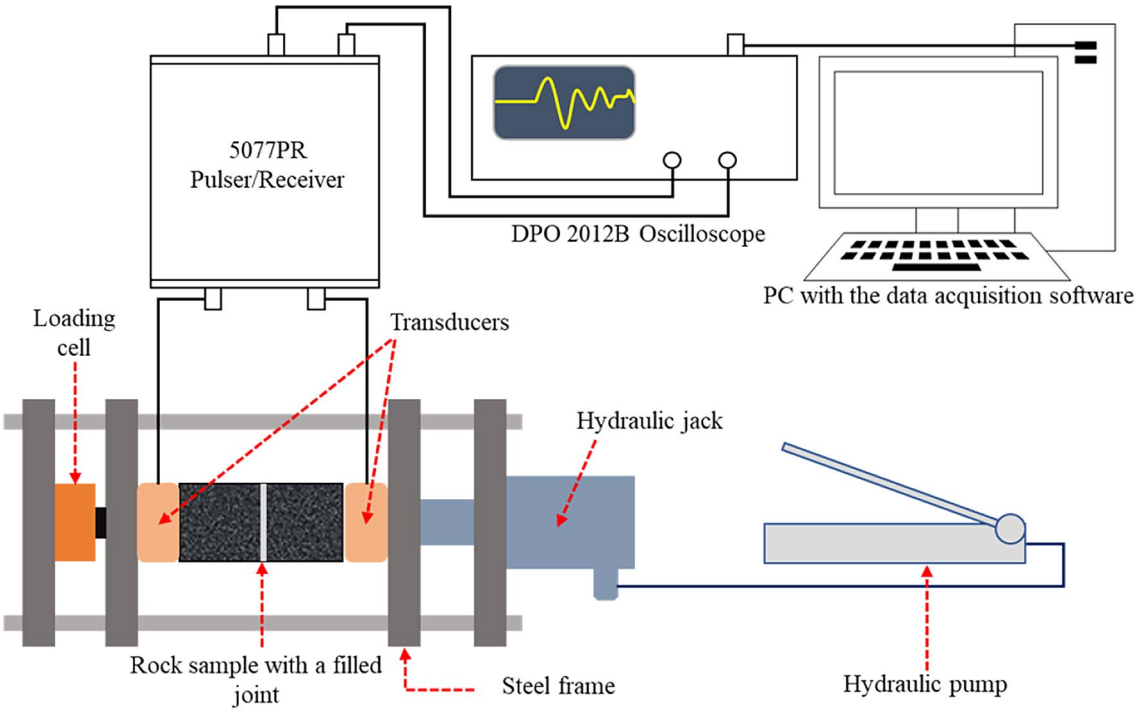

Fig. 2 The schematic of the self-developed ultrasonic test configuration for this study

Table 2 Information about the waves collected from the tests on the intact gabbro rock specimen

The transducer pair model	f_d (MHz)	f_R (MHz)	V_R (m/s)	λ (mm)
V150	0.25	0.229	3424.16 ± 11.27	14.953 ± 0.049
V151	0.5	0.473	3603.87 ± 2.94	7.619 ± 0.006
V152	1	0.595	3846.244 ± 15.37	6.414 ± 0.026

f_d represents the default central frequency of signals emitted by the S-wave transducers that the manufacturer provides. f_R is the central frequency of transmitted S-waves across the intact gabbro rock reference. V_R represents the S-wave velocity across the intact gabbro rock reference. λ stands for the wavelength of S-waves in the intact gabbro rock

The face-to-face tests were conducted to calibrate the test configuration and the transducer pairs (ASTM Standard D-18 2008). After the calibration, three sets of ultrasonic tests were performed on rock specimens using three transducer pairs with different central frequencies in sequence. In each group, eight cases were tested, including seven clay-rich fractured rock specimens and an intact reference specimen, and five repetitions were conducted for each case. Accordingly, 120 ultrasonic tests in total were performed. For each ultrasonic measurement, two transducers and a rock specimen sandwiched between them were placed in the steel supporting frame (Fig. 2). A constant axial stress (i.e., 0.197 MPa) was imposed via the hydraulic jack. A specified couplant (i.e., Olympus SWC-2) was applied to the rock-transducer interfaces to make them well coupled. Two S-wave transducers attached to the end surfaces of the rock sample should be in line with each other to ensure the alignment of polarization. During the measurement, one transducer connected to the Pulser/Receiver converted square signals with 200 V in amplitude and 1×10^{-5} s in length into input waves at the transducer-specific central frequencies. The transmitted waves passing through the tested rock specimen were received by the other transducer connected to the Pulser/Receiver and then digitally displayed and recorded in the oscilloscope. For each test, 64 signals were stacked and averaged by the oscilloscope to achieve a high signal-to-noise ratio. The collected waveforms were saved on the PC connecting to the oscilloscope for further data processing and analysis.

2.3 Data Processing Methods

The S-wave velocity across single clay-rich rock fractures can be calculated via (Fratta and Santamarina 2002)

$$V_F = d/\left(t - L_R/V_R\right), \tag{1}$$

where d is the fracture thickness; t is the travel time of S-waves across the fractured rock specimen; L_R is the length of the host rock; V_R is the S-wave velocity across the host rock. V_R is obtained from the received S-waves across the

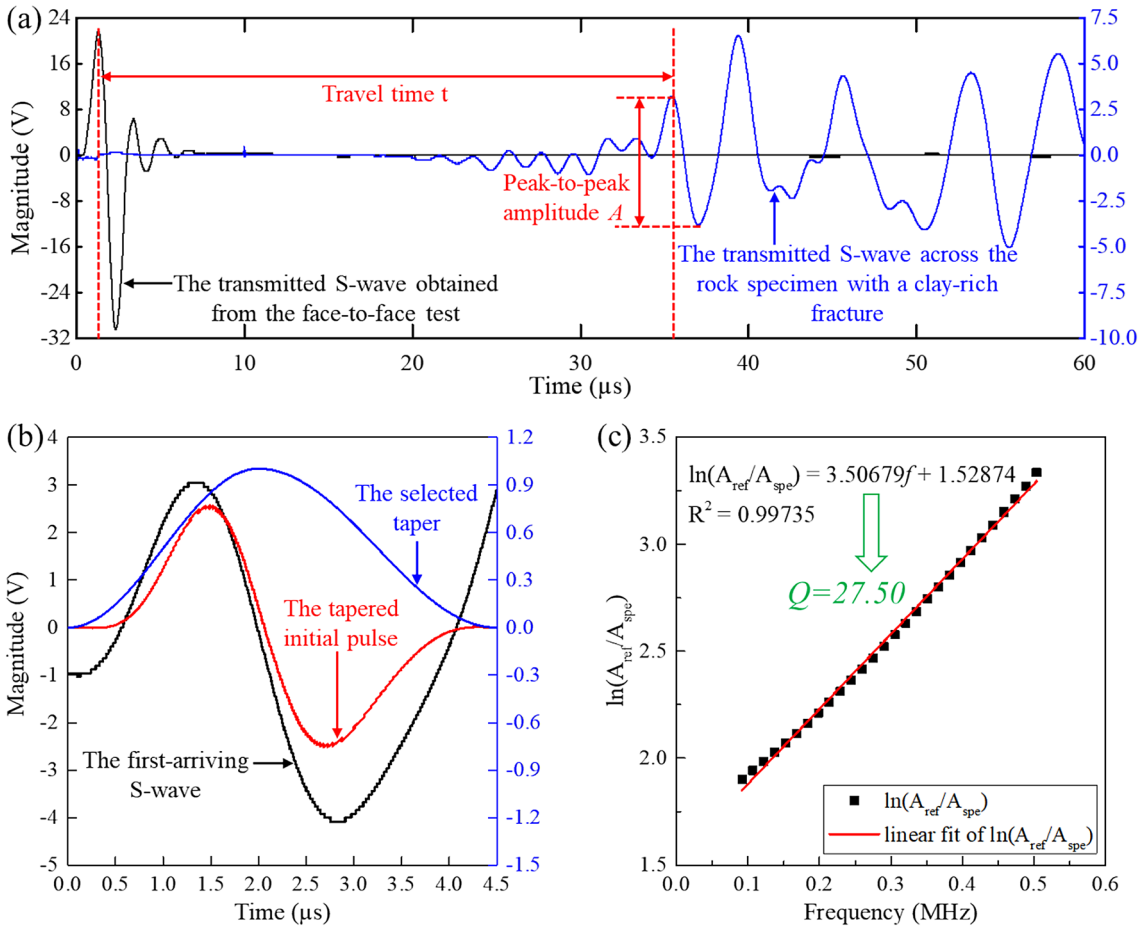

Fig. 3 Illustration of wave analyzing process for this study based on a dataset for the 0.5-MHz incident S-wave passing across the clay-rich rock fracture at the water saturation of 80%: **a** determination of the travel time of the S-wave; **b** extraction of the initial transmitted S-wave via the tapering; and **c** calculation of the *Q* values using the linear fitting

intact gabbro reference. The travel time of S-waves across the tested rock specimen is determined using the time difference between the first peak of the calibration signal and the corresponding peak of the transmitted S-wave across the tested sample (Fig. 3a). This travel-time picking method effectively eliminates the distortion caused by the near-field effect and provides a reasonably good estimation of group velocity (Molyneux and Schmitt 2000; Viggiani and Atkinson 1995).

The frequency spectra of the transmitted S-waves are obtained by performing the fast Fourier transform (FFT) on the first-arrival parts extracted from those original pulses via the proper window functions (i.e., the tapers). The appropriate tapers are selected via trial and error according to the criteria for preserving more low-frequency components and distorting less high-frequency modes of the original waveforms (Pyrak-Nolte et al. 1990). Figure 3b illustrates a typical tapering of an original waveform. Note that, for tests using the same incident S-waves, the received signals should be tapered using the same taper to ensure that the results of the FFT processing are consistent and directly comparable to each other. For all selected tapers, the amplitude is unity, and the width coincides with the duration of the first-arrival pulse.

Wave attenuation in rock masses is commonly quantified using the seismic quality factor Q calculated via the spectral ratio technique presented by Toksoz et al. (1979). In the spectral ratio method, wave attenuation coefficient α is assumed as a linear function of frequency and inversely related to the seismic quality factor Q (i.e., $\alpha = \pi f/QV$) (Toksoz et al. 1979). Besides, the geometric factors of the sample and reference with the same dimensions are assumed to have the same frequency dependence (Toksoz et al. 1979). For incident plane waves, the natural logarithm of the spectral amplitude ratio of the reference signal to the transmitted pulse across the tested specimen can be expressed as (Bourbie and Zinszner 1985)

$$\ln\left(A_1/A_2\right) = -\pi L\left[\left(1/Q_1V_1\right) - \left(1/Q_2V_2\right)\right]f, \tag{2}$$

where A is the spectral amplitude; Q is the seismic quality factor; V is the wave velocity; L is the length of the specimen; f is the frequency. The subscripts 1 and 2 denote the reference and the tested sample, respectively. Conventionally, the aluminum cylinder with identical dimensions to the tested rock specimens is used as the standard reference (Bourbie and Zinszner 1985). For aluminium as a reference, it is assumed that $1/Q_1 \simeq 0$. Thus, Eq. (2) can be simplified as

$$\ln\left(A_1/A_2\right) = \pi Lf/Q_2V_2. \tag{3}$$

From Eq. (3), the seismic quality factor Q_2 of the tested specimen can be determined from the slope of a linear fit of $\ln\left(A_1/A_2\right)$ versus f (Fig. 3c).

3 Results and Analyses

3.1 Water Effect on S-Wave Velocity Across Single Clay-Rich Rock Fracture

The S-wave velocity across single clay-rich rock fractures is plotted as a function of the water saturation degree in Fig. 4. It is shown that S-wave velocity slightly increases and then decreases with continuously rising water saturation. More specifically, S-wave velocity across the clay-rich rock fracture increases by around 1.6%, 1.8%, and 3.0% for S-waves at the default central frequency of 0.25-MHz, 0.5-MHz, and 1-MHz, respectively, as the degree of water saturation increases from 48 to 64%. When the water saturation degree rises from 64 to 96%, S-wave velocity across the clay-rich fracture decreases by about 3.0%, 1.1%, and 1.6% for S-waves at the default central frequency of 0.25-MHz, 0.5-MHz, and 1-MHz, respectively. The higher the default central frequency of S-waves, the lower the S-wave velocity across single clay-rich rock fractures.

3.2 Water Effect on Frequency Spectra of S-Wave Across Single Clay-Rich Rock Fracture

Figure 5 presents the frequency spectra of transmitted S-waves calculated using the method described in Sect. 2.3. The central frequency and corresponding peak amplitude of these frequency spectra are then summarized in Table 3. Compared to the intact rock reference, rock specimens

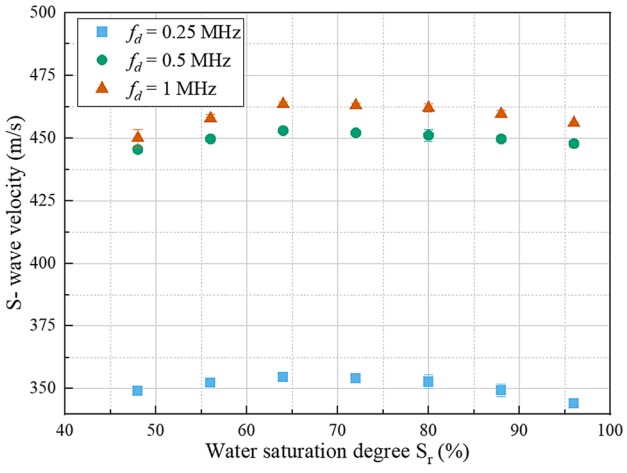

Fig. 4 S-wave velocities across single clay-rich rock fractures versus the water saturation degree

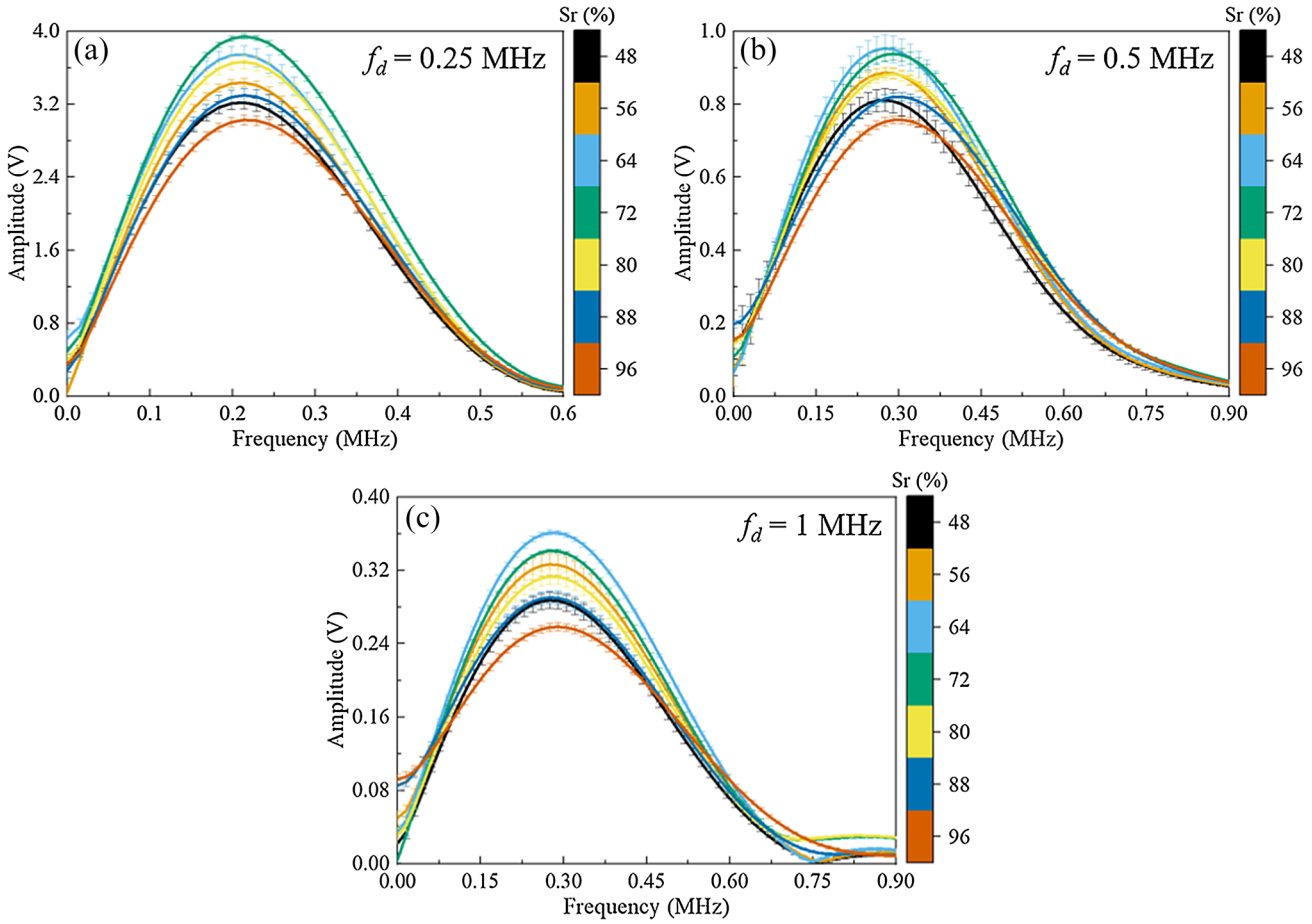

Fig. 5 Frequency spectra of transmitted S-waves across single clay-rich rock fractures at the default central frequencies of **a** 0.25 MHz, **b** 0.5 MHz, and **c** 1 MHz

Table 3 Central frequencies (f_c) and peak amplitudes (A) obtained from the frequency spectra for all tested rock specimens

	0.25-MHz S-wave		0.5-MHz S-wave		1-MHz S-wave	
	f_c (MHz)	A (V)	f_c (MHz)	A (V)	f_c (MHz)	A (V)
Intact rock specimen	0.229	13.051 ± 2.282	0.473	8.219 ± 1.047	0.595	4.153 ± 0.591
Fractured rock specimen containing CG-1	0.214	3.218 ± 0.079	0.275	0.811 ± 0.031	0.275	0.287 ± 0.009
Fractured rock specimen containing CG-2	0.214	3.436 ± 0.063	0.275	0.887 ± 0.019	0.275	0.326 ± 0.013
Fractured rock specimen containing CG-3	0.214	3.744 ± 0.100	0.275	0.953 ± 0.059	0.275	0.361 ± 0.013
Fractured rock specimen containing CG-4	0.214	3.942 ± 0.044	0.290	0.938 ± 0.031	0.275	0.341 ± 0.006
Fractured rock specimen containing CG-5	0.214	3.664 ± 0.063	0.290	0.882 ± 0.013	0.275	0.313 ± 0.008
Fractured rock specimen containing CG-6	0.214	3.297 ± 0.077	0.290	0.820 ± 0.011	0.275	0.290 ± 0.009
Fractured rock specimen containing CG-7	0.214	3.027 ± 0.052	0.305	0.757 ± 0.010	0.290	0.258 ± 0.007

containing single clay-rich fractures exhibit lower central frequencies and smaller peak amplitudes of transmitted S-waves. Specifically, the presence of clay-rich rock fractures causes a decrease in the central frequency of about 6.6%, 38.6%, and 53.8% for propagating S-waves at the default central frequency of 0.25 MHz, 0.5 MHz, and 1 MHz, respectively. In addition, because of clay-rich rock fractures, the peak amplitude reduces by a factor of about 4, 10, and 14 for transmitting S-waves at the default central frequency of 0.25 MHz, 0.5 MHz, and 1 MHz, respectively. Independent of the default central frequency of incident S-waves, water saturation strongly affects the spectral amplitudes but moderately influences the central frequency of the transmitted S-wave across single clay-rich rock fractures

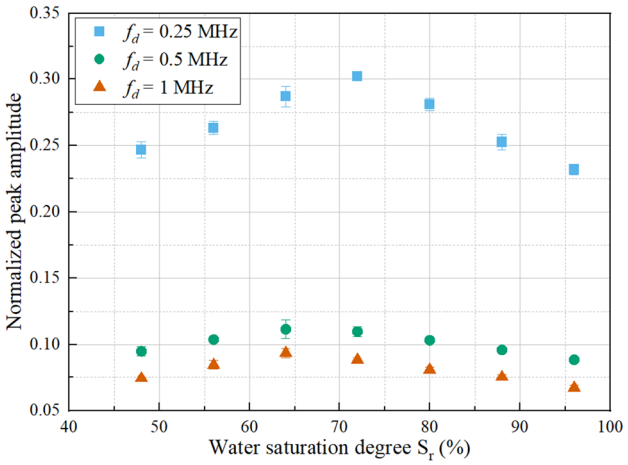

Fig. 6 Normalized peak amplitudes of transmitted S-waves across single clay-rich rock fractures versus the degree of water saturation

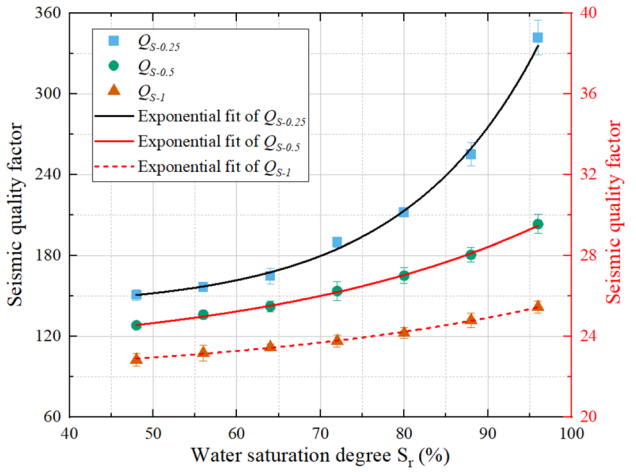

Fig. 7 The seismic quality factor for S-wave propagation across single clay-rich rock fractures versus the water saturation degree of filling clay-rich gouges at different default central frequencies of 0.25 MHz, 0.5 MHz, and 1 MHz. $Q_{S-0.25}$, $Q_{S-0.5}$, and Q_{S-1} represent the seismic quality factor for 0.25-MHz, 0.5-MHz, and 1-MHz S-waves, respectively. Note that the left y-axis (black) was used for $Q_{S-0.25}$ (black curve), while the right y-axis (red) was used for $Q_{S-0.5}$ and Q_{S-1} (red curves). (Colour figure online)

(Fig. 5 and Table 3). The central frequencies of the transmitted S-waves slightly shift towards higher values as the water saturation degree of single clay-rich rock fractures increases for the incident 0.5- and 1-MHz S-waves, while it remains almost unchanged with the increasing water saturation for the 0.25-MHz incident S-waves. By contrast, the peak amplitudes of S-waves transmitting across single clay-rich rock fractures increase initially and then decrease upon rising water saturation.

To further specify the influence of water saturation on spectral amplitudes of transmitted S-wave across single clay-rich rock fractures, we normalize the peak amplitudes for the fractured rock specimens by dividing their values by that for the intact rock specimen. Figure 6 presents the normalized peak amplitudes versus the water saturation degree for S-waves at different default central frequencies. The normalized peak amplitudes exhibit a concave tendency upon rising water saturation degree, irrespective of the default central frequency of incident S-waves. The critical water saturation degree where the normalized peak amplitude maximizes slightly shifts from 72 to 64% as the default central frequency increases from 0.25 to 1 MHz. The higher the default central frequency, the lower the normalized peak amplitude. Over the tested water saturation range, the normalized peak amplitude for 0.25-MHz S-wave is 2.1–3.4 times and 2.3–4.5 times of that for 0.5-MHz and 1-MHz S-waves, respectively.

3.3 Water Effect on Attenuation of S-Wave Across Single Clay-Rich Rock Fracture

The seismic quality factor of S-waves (Q_S) obtained using Eq. (3) is plotted as a function of the water saturation degree (S_r) in Fig. 7. Irrespective of the default central frequency of incident S-waves, Q_S monotonically increases with S_r in a nonlinear form. That is, S-wave attenuation nonlinearly decreases with increasing water saturation. The lower the default central frequency of S-waves, the larger the Q_S at a specific S_r, and the more significant the increase in Q_S upon rising S_r. Specifically, the values of Q_S for 0.25-MHz S-waves are about one order larger than those for 0.5-MHz and 1-MHz S-waves at a given S_r. In other words, clay-rich rock fractures cause more energy attenuation for S-waves at higher frequencies. Besides, Q_S increases by about 118.4%, 17.8%, and 9.8% for 0.25-MHz, 0.5-MHz, and 1-MHz S-waves, respectively, as S_r increases from 56 to 96%. That means the attenuation for S-waves at lower frequencies is more sensitive to varying water saturation of clay-rich rock fractures.

We also perform the curve-fitting analysis of the relationship between Q_S and S_r using the least square regression method, which gives an exponential model as below

$$Q_S = Q_0 + a * \exp\left(b * S_r\right), \tag{4}$$

where the intercept Q_0 could be physically defined as the seismic quality factor at zero water saturation degree (i.e., the dry clay-rich gouge); a and b are the specific constants. The values curve-fitting parameters and the correlation coefficients (R^2) for S-waves at different default central frequencies are summarized in Table 4. The values of R^2 are greater than 0.99 for all tested S-waves, indicating that the exponential Q_S–S_r model fits the test results very well for this

Table 4 Curve-fitting parameters (Q_0, a and b) and correlation coefficients (R^2) of the exponential Q_S–S_r model for the incident S-waves at different default central frequencies (f_d)

f_d (MHz)	Q_0	a	b	R^2
0.25	140.865	0.515	0.062	0.992
0.5	22.964	0.398	0.029	0.998
1	21.883	0.298	0.026	0.997

study. Q_S exponentially increases with S_r as S-waves propagate across single clay-rich rock fractures. In other words, an exponentially decreasing relationship exists between S-wave attenuation and the water saturation degree of rock fractures filled with the kaolinite-dominant gouge.

3.4 Comparison of S- and P-Wave Behaviours Across Single Wet Clay-Rich Rock Fractures

Our preliminary work has determined P-wave attributes across single rock fractures filled with wet kaolinite-dominant gouges (Yang et al. 2023). Herein, we compare the previously estimated P-wave signatures to S-wave properties measured by this experiment in terms of wave velocity, central frequency, normalized peak amplitude, and seismic quality factor (Fig. 8). Note that the default central frequency for incident P- and S-waves is 1 MHz. The differences between S-wave and P-wave attributes are demonstrated below.

1. Both P- and S-wave velocities display a concave trend upon increasing water saturation (Fig. 8a). The inflection of wave velocity occurs at the water saturation degree of around 64% and 80% for S- and P-wave, respectively. In addition, P-wave velocity varies in the range of 1043.71–1126.00 m/s, while S-wave speed ranges from 450.00

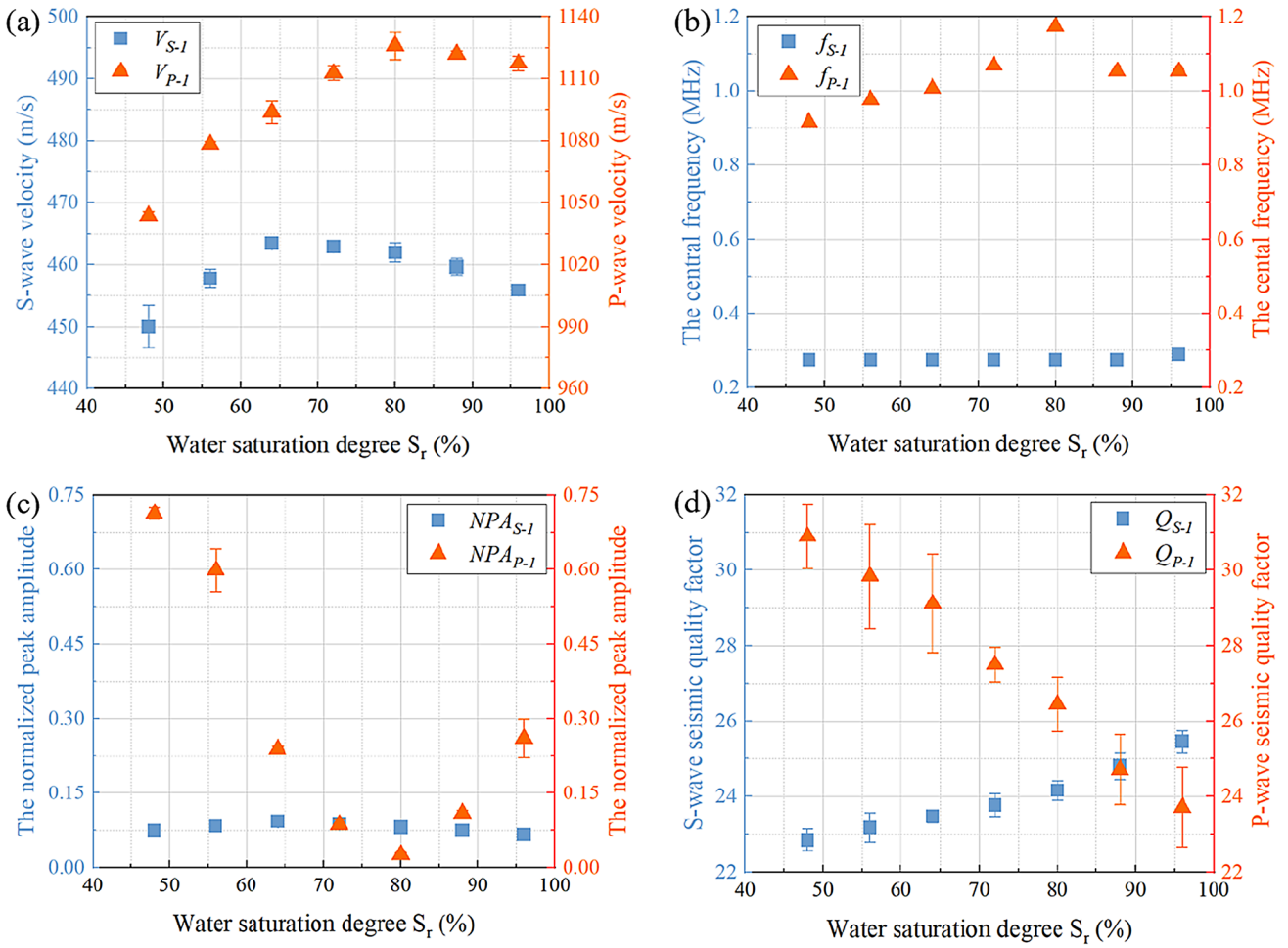

Fig. 8 Comparison between P- and S-wave attributes across single water-saturated clay-rich rock fractures: **a** wave velocity, **b** peak frequency (f), **c** normalized peak amplitude (NPA), and **d** seismic quality factor (Q). Note that the subscripts (P-1) and (S-1) denote 1-MHz P- and S-waves, respectively

to 463.50 m/s as the water saturation degree increases (Fig. 8a). It indicates that P-wave velocity is more sensitive to varying water saturation compared to S-wave velocity.

2. The central frequency for transmitted P-waves exhibits a concave tendency upon rising water saturation, which is consistent with the evolution of P-wave velocity (Fig. 8b). By comparison, the central frequency for transmitted S-waves slightly changes as water saturation increases. The central frequency for P-waves, ranging from 0.9 to 1.2 MHz, is much higher than that for S-waves at about 0.28 MHz (Fig. 8b). It means that the central frequency shift for P-waves is much more sensitive to varying water saturation than for S-waves.
3. The normalized peak amplitude for P-waves displays a convex trend upon rising water saturation (Fig. 8c). The evolution of the normalized peak amplitude for S-wave is approximately opposite to that for P-waves (Fig. 8c). Figure 8c also shows the normalized peak amplitude for P-wave is generally greater than that for S-waves at a given saturation level. Besides, the variation in the normalized peak amplitude for P-wave is more significant than that for S-wave upon rising water saturation (Fig. 8c).
4. The seismic quality factor for 1-MHz P-wave ($Q_{P\text{-}1}$) monotonically decreases upon increasing water saturation, which is reverse to the evolution of the seismic quality factor for 1-MHz S-wave ($Q_{S\text{-}1}$) (Fig. 8d). The value of $Q_{S\text{-}1}$ is generally smaller than that of $Q_{P\text{-}1}$, indicating the attenuation of the S-wave is greater than that of P-waves in most circumstances.

4 Discussion

4.1 Saturation Dependence of S-Wave Behaviours Across Single Water-Saturated Clay-Rich Rock Fractures

Our measurements indicate that S-wave velocity across single clay-rich rock fractures displays a concave tendency upon rising water saturation degree. The increase in S-wave velocity can be mainly attributed to the local flow effect. As waves propagate across clay-rich rock fracture, the passing waves could deform the micro-cracks/pores and produce a local pressure gradient that causes pore fluids to flow from the more compliant regions to the less compliant areas (Khazanehdari and Sothcott 2003). The wave-induced fluid flow has insufficient time to equilibrate during the one-half period of the wave cycle for high-frequency propagating waves (e.g., ultrasonic waves in this study). Thus, pore fluids in the compliant regions are trapped, reinforcing the compliant parts and improving the apparent stiffness of those zones, which is the so-called local flow effect (Mavko and Jizba 1994). With the increasing saturation, more water is accumulated within the compliant regions (Fig. 9). Accordingly, the stiffening of those areas due to the local flow effect becomes more significant, causing a larger effective shear

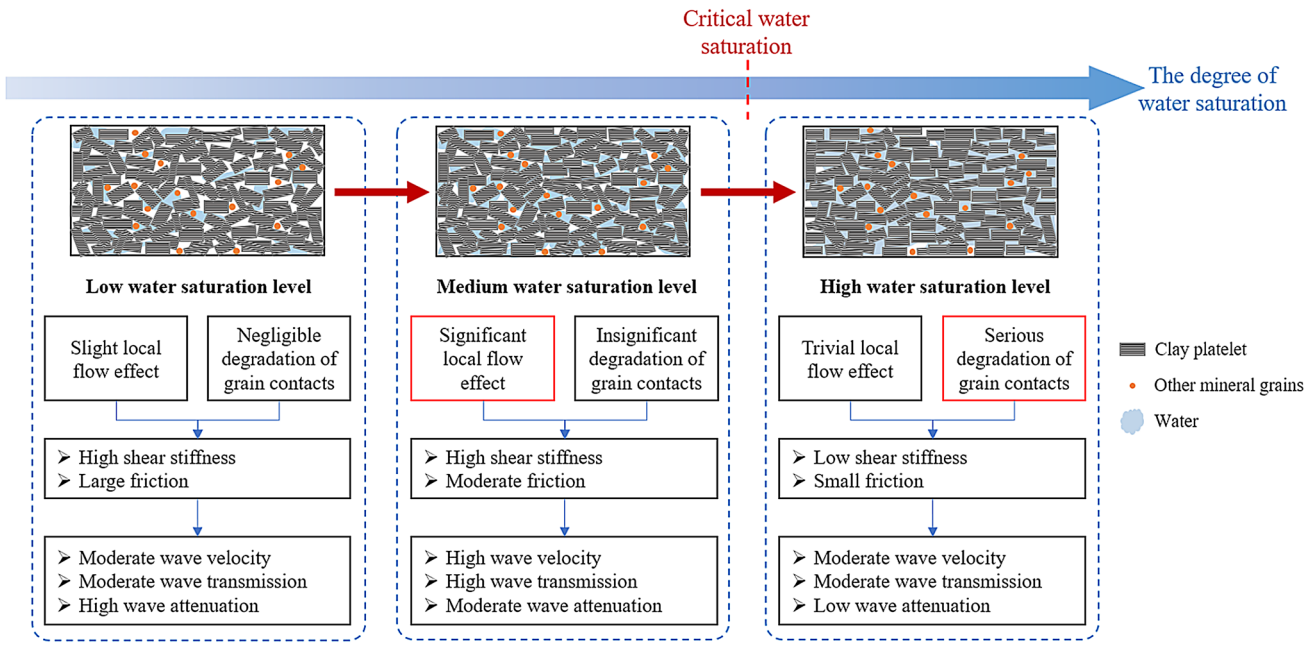

Fig. 9 Schematic illustration of possible physical mechanisms for water effects on S-wave responses to single clay-rich rock fractures. The red rectangle highlights the dominant role played by the specific factor in S-wave propagation across clay-rich rock fractures

modulus and faster S-wave velocity across the clay-rich rock fracture (Kaproth and Marone 2014; Li et al. 2018). Besides, the decrease in bulk density caused by rising water saturation (Table 1) could partly contribute to the increase in S-wave velocity. On the other hand, the reduction in S-wave velocity at high water saturation degrees is primarily due to the dramatic weakening of the clay-rich gouge skeleton, which is supported by the decreasing shear modulus measured by the amplitude sweep tests (Table 1). Specifically, overwhelming water saturation enhances the hydration of clay, consuming more surface energy and thus weakening grain-to-grain contacts (Atkinson 1984; Li et al. 2020). Meanwhile, the higher the degree of water saturation, the less the matric suction (i.e., capillary forces) generated by the development of water menisci at the particle contacts, and the smaller the interparticle contact forces in the clay-rich gouge (Cho and Santamarina 2001). Therefore, at high water saturation degrees, the grain contacts gradually weaken upon rising water saturation, dominating the effective stiffness of clay-rich rock fracture and thus reducing S-wave velocity (Fig. 9).

We find that the increased water saturation modestly influences the central frequency and leads to a concave trend of the peak amplitude of transmitted S-waves. The central frequency seems unchanged in the water saturation range of 48–88%, while a minor increase in the central frequency of S-wave is observed at the water saturation degree of 96%. It is probably because fluid distribution in the clay-rich rock fracture is homogenous at such a high-water saturation degree (i.e., 96%), reducing the wave dispersion caused by the fluid movement (Carcione et al. 2003). In addition, the peak amplitude exhibits a similar concave tendency with the S-wave velocity, indicating that transmitted S-wave energy increases at first and then decreases upon increasing water saturation. We ascribe this finding to the trade-off between the local flow effect and the weakening of the clay-rich gouge skeleton (Khazanehdari and Sothcott 2003). The variation in the peak amplitude ranges from 1.1 to 25.8%, which is much larger than that in the central frequency. It suggests that, compared to the frequency, the spectral amplitude is more sensitive to varying water saturation.

This study also shows that the values of Q_S increase exponentially with rising S_r. It indicates that S-wave attenuation decreases with the water saturation of the clay-rich rock fracture. The principal explanation is that water saturation weakens the grain-to-grain contacts and reduces the viscous drags between clay particles, causing less frictional energy loss due to relative motions between grains (Wang et al. 2021; Zhu et al. 2011). Alternatively, the porosity of the clay-rich gouge layer decreases upon increasing water saturation, reducing wave scattering and contributing to the decrease in the overall wave attenuation. The exponential relation between Q_S and S_r indicates that S-wave energy dissipation decreases at an increasing rate. It is likely because the higher the water saturation, the more the reduction in viscous friction, the weaker the local flow effect, and thus the greater the decline in the overall S-wave attenuation.

The above discussion suggests that water effects on S-wave behaviours across single clay-rich rock fracture are governed by the local flow effect and grain-to-grain contacts, which are directly dependent on the physicochemical interaction of water with the kaolinite-dominant gouge (Fig. 9). The water-kaolinite interaction is dominated by the particle surface hydration, where the oxygen/hydroxyl anions at the particle surface can attract the hydrogen cation toward them (Aksu et al. 2015). The hydration of kaolinite has a weak softening effect on the frame of the clay-rich gouge layer. The kaolinite-dominant gouge comprises elementary crystalline aggregates and micropores (Moyano et al. 2012). The absorbed water tends to displace the air in the formerly existing pores at first and thus enhances the cohesion of the kaolinite-dominant gouge; then, the overwhelming water saturation deteriorates the cementation bonds between particles and thus reduces the shear resistance of the kaolinite-dominant gouge (Li et al. 2020). Accordingly, fluid distribution in the kaolinite-dominant gouge gradually transfers from a heterogeneous state into a homogeneous mode upon increasing water saturation. The grain-to-grain contacts become weaker with water saturation, which manifests as decreases in the shear modulus and viscosity (Table 1). Over the tested water saturation range, the local flow effect first dominates the effective elastic moduli of clay-rich gouges; after reaching the critical water saturation, the weakening of grain-to-grain contacts plays a controlling role. Therefore, we suggest that the physicochemical interaction of water with the kaolinite-dominant gouge is the first-order physical mechanism for water effects on S-wave attributes across single clay-rich rock fracture.

4.2 Frequency Dependence of S-Wave Behaviours Across Single Water-Saturated Clay-Rich Rock Fractures

Our experiments reveal that S-wave attributes across single clay-rich rock fractures rely on the default central frequency of incident waves. Specifically, the higher the central frequency of S-waves, the faster the wave velocity and the larger the energy dissipation across single clay-rich rock fractures. One reason is that the stiffening effect caused by the local flow becomes more pronounced with increasing frequency (Cadoret et al. 1995). The path dispersion mechanism suggests that high-frequency wave components prefer to propagate along incompressible, high-speed regions for wave propagation through a heterogeneous medium with high and low-compressible areas (Adam et al. 2009). Accordingly, propagating S-waves at higher frequencies

enhance the stiffening of compliant pores in clay-rich gouge, providing more paths for high-frequency wave modes to pass and thus increasing S-wave velocity across the clay-rich rock fracture. Besides, the relative motions between fluid and solid become more intense with the reinforced local flow, causing more energy dissipation during the propagation of S-waves. The scattering caused by the microporosity of the clay-rich rock fracture could be another possible reason for the frequency dependence of S-wave behaviours. S-waves at higher frequencies can interact with more micro-scale heterogeneities because of their shorter wavelength. As a result, more significant scattering occurs at higher frequencies, causing more energy dissipation. Another explanation for the frequency-dependent transmitted wave energy could be that the wave impedance contrast between the host rock and the clay-rich fracture increases with the wave frequency (Zhu et al. 2011). The greater the wave impedance contrast between the host rock and the fracture, the less the transmitted wave energy across the clay-rich fracture (Zhu et al. 2011).

Our results also indicate less frequency dependence of S-wave properties across water-saturated clay-rich rock fractures at higher frequencies (Figs. 4, 6). It is consistent with previous experimental findings and theoretical predictions of S-wave propagation across fluid-saturating porous media, which is known as wave dispersion (Tuncay and Yavuz Corapcioglu 1996; Denneman et al. 2002; David et al. 2013; Pimienta et al. 2016). The general wave dispersion curve estimated by theoretical models shows that wave velocity is small and stable in the low-frequency band and then increases as the frequency increases, finally converging to a constant value in the high-frequency band. Unfortunately, no clear experimental evidence of these distinct regimes of frequency behaviours has been given so far. Upon acoustic excitation, saturating fluids are subject to local (i.e., pore scale) fluid flow whose intensity depends on the size of the pore throats for a given frequency, which is increasingly believed to be the driving mechanism behind the frequency dependence of wave dispersion (Pride et al. 2004; Müller et al. 2010).

4.3 Possible Mechanisms for Discrepancies Between S- and P-Wave Behaviours Across Single Water-Saturated Clay-Rich Rock Fractures

The comparison between S- and P-wave signatures across single water-saturated clay-rich rock fractures reveals that the inflection of wave velocity takes place at a higher water saturation for P-wave rather than S-wave (Fig. 8a). It is likely because the local flow effect positively impacts the bulk modulus more than the shear modulus of compliant regions. In other words, substituting air with water distinctly improves the effective bulk modulus of the clay-rich gouge layer but has a modest effect on shear modulus since water does not support shear waves.

Figure 8b illustrates that the central frequency for P-waves (0.9–1.2 MHz) is much higher than that for S-waves (~ 0.28 MHz). This is mainly because the deterioration of grain contacts due to water addition significantly reduces the shear resistance of clay-rich gouges. The decreasing shear modulus measured by the amplitude sweep tests is an indicator of the reduction in shear resistance (Table 1). We also find that increasing water saturation causes an obvious central frequency shift for P-waves while it has a modest effect on the central frequency of S-waves. That wave-induced local flow exerts more significant influences on the bulk modulus than the shear modulus of clay-rich rock fracture can explain this finding.

Figure 8c uncovers that the tendency of S-wave transmission is approximately opposite to that of P-wave transmission as water saturation continuously increases. For incident P-waves, increasing water content firstly enhances the local fluid flow and thus causes more energy dissipation, significantly reducing wave transmission. After reaching the critical water saturation, the inhibited local flow and the weakened friction between particles induced by increasing water saturation leads to less P-wave attenuation and more P-wave transmission. For incident S-waves, the viscous drag between particles decreases upon increasing water saturation, reducing the friction energy loss and improving the transmission of S-wave. Beyond the critical water saturation, the degradation of grain contacts causes a significant decrease in the shear modulus, overpowering the effect of friction loss and reducing S-wave transmission. Our inferences are partly verified by the decreasing viscosity and shear modulus measured by amplitude sweep tests (Table 1). Besides, the greater normalized peak amplitude for P-waves rather than S-waves at a given saturation level suggests that water-saturated clay-rich rock fractures generally allow more P-wave energy to transmit, consistent with observations of some porous rocks (Lucet and Zinszner 1992).

The seismic quality factor for 1-MHz P-wave ($Q_{P\text{-}1}$) monotonically decreases upon increasing water saturation, indicating that P-wave energy dissipation increases with water saturation (Fig. 8d). We attribute this to the relative motion between the gouge skeleton and water caused by the wave-induced local flow. On the contrary, the rising water saturation causes an increase in the seismic quality factor for 1-MHz S-wave ($Q_{S\text{-}1}$), suggesting a reduction in S-wave energy dissipation (Fig. 8d). It is likely due to the increasing water saturation weakens the viscous drags between clay particles, reducing S-wave energy attenuation. The weakening viscous drag is manifested as the reduction in the viscosity measured by the amplitude seep tests (Table 1). Figure 8d also reveals that the attenuation of the S-wave is generally greater than that of P-waves, in agreement with theoretical

predictions reported by Pham et al. (2002). A plausible explanation is that the S-wave wavelength (about 0.46 mm) is much shorter than the P-wave wavelength (about 1.1 mm). Thus, more scattering caused by micro-defects occurs for the propagation of S-waves, resulting in high attenuation (Johnston et al. 1979). Another possible reason is that the ultrasonic S-wave entering the anisotropic clay-rich rock fracture tends to separate into two polarized modes with different propagating velocities. These two split phases are combined at the other side of the fracture into another shear wave with a different waveform (i.e., different frequency contents and amplitudes) from the incident wave, leading to strong external attenuation of S-waves (Auld and Green 1974).

Figure 8a and c demonstrate a difference in the critical water saturation for the evolution of P- and S-wave attributes across single clay-rich rock fractures. Based on existing relevant studies (Winkler and Nur 1982; Mavko and Jizba 1991; Moyano et al. 2012), we infer that the difference in critical water saturation between P- and S-waves could be attributed to the saturation and geometry of microcracks/pores in the clay-rich gouge layer. Specifically, the geometry and saturation of microcracks/pores significantly affect elastic moduli and wave-induced fluid flow, thereby dominating P- and S-wave velocity and transmission. For partially saturated cracks, bulk compression causes every crack to be compressed and contributes to fluid flow and/or thermoelastic energy losses; in contrast, pure shear makes some cracks oriented such that there is no normal stress on the crack surface, and thus these cracks will not be compressed and will not contribute to energy loss (Winkler and Nur 1982). This implies that fluid flow behaviours in the clay-rich rock fracture during the propagation of the P-wave are different from those during the passing of the S-wave. The shear stiffness highly depends on the small aspect-ratio defects (i.e., elongated pores), while the bulk modulus seems to be controlled by large aspect-ratio defects (i.e., more rounded pores) (Mavko and Jizba 1991). The topology of kaolinite from SEM image analysis has shown that platelets stacked together as a deck of cards, forming particles or clusters with elongated pores between them, and the interaggregate pores in the kaolinite exhibit a slight but visible preferential orientation (Moyano et al. 2012). This is why the local fluid flow behaves in different patterns under the excitation of P- and S-waves, respectively.

The discrepancies between P- and S-wave signatures confirm that S-wave attributes across single water-saturated clay-rich rock fractures mainly depend on the properties of the skeletal frame (Leurer 1997). In contrast, P-wave behaviours across single water-saturated clay-rich rock fractures are governed by the features of the particles, pore fluid, and skeleton (Leurer 1997). The particle size of kaolinite-dominant gouge used in this study is approximately 0.01 mm (Yang et al. 2023). The value is much smaller than the wavelength of P- and S-waves, which are about 1.1 mm and 0.46 mm, respectively. Therefore, the effect of particle size can be safely neglected for this study.

5 Conclusions

This study quantitatively examines the water effects on S-wave propagation and attenuation across single rock fractures filled with kaolinite-dominant gouges based on systematic laboratory ultrasonic measurements. The experimental results show that S-wave velocity across single clay-rich rock fractures slightly increases at first and then decreases with increasing water saturation. The increased water saturation modestly affects the central frequency for S-waves across single clay-rich rock fractures. By comparison, the spectral amplitude of transmitted S-waves exhibits a concave tendency as water saturation increases. Moreover, a solid exponential growth relationship exists between the seismic quality factor for S-waves and the water saturation degree, indicating that S-wave attenuation exponentially decreases with water saturation. Compared to wave velocity and central frequency, S-wave energy transmission and dissipation are more sensitive to varying water saturation degrees of single clay-rich rock fractures. We attribute the evolution of S-wave attributes across single wet clay-rich rock fractures to the combined effects of the local flow and the degradation of grain contacts. Our measurements also reveal the dependence of elastic S-wave signatures across single clay-rich rock fractures on wave frequency. The higher the S-wave frequency impinging upon single clay-rich rock fractures, the higher the wave velocity, the less the wave energy transmission, and the more the wave dissipation. We interpret these findings from perspectives of the path effect, wave scattering, and wave impedance contrast.

We compare the responses of 1-MHz S-wave to those of P-wave to single clay-rich rock fractures at different water saturations. Both P- and S-wave velocity changes in a concave form with rising water saturation, but the critical water saturation degree corresponding to inflection points is higher for P-waves than S-waves. The increased water saturation moderately influences the central frequency for S-waves but leads to a concave tendency of the central frequency for P-waves. The peak amplitude of transmitted P-waves exhibits a convex trend, which is contrary to the variations in the peak amplitude of transmitted S-waves. S-wave attenuation exponentially decreases while P-wave attenuation monotonically increases upon increasing water saturation. We infer that these discrepancies are due to the fact that S-wave attributes across single water-saturated clay-rich rock fractures mainly depend on the properties of the skeletal frame, while the characteristics of the particles, pore fluid, and skeleton frame dominate P-wave behaviours.

This study provides extensive laboratory data for further understanding the physical mechanisms behind the saturation-dependent elastic wave signatures across clay-rich rock fractures from the viewpoint of the combined effects of local flow and the degradation of grain-to-grain contacts. Moreover, the present study suggests that the S-wave attributes appear to be strong indicators of the degree of water saturation in clay-rich rock fractures. Our experimental results may have good potential for developing a means of noninvasively estimating and monitoring the water saturation conditions of clay-rich rock fractures. Besides, the findings could be beneficial in interpreting seismic wave behaviours observed from field investigations of rock fractures. Nevertheless, our observations are limited to rock fractures at a steady state that lacks possible co-seismic processes commonly encountered in nature. Therefore, more careful laboratory experiments are necessary to obtain insights into the fluid effects on wave responses to clay-rich rock fractures subjected to in-situ loadings. In addition, more investigations are needed to determine how the mineral constituents and the saturating fluid properties alter S-wave behaviours across clay-rich rock fractures.

Acknowledgements The financial support from RGC projects [no. 15202122] (Hong Kong Government) is gratefully acknowledged. Dr. H. Yang is supported by the Joint Postdoc Scheme with Non-local Institutions by PolyU (P0042945). The authors appreciate Prof. Yuhong WANG for his guidance in analyzing the rheological properties of clayey soils and Mr. Xingyu CHEN and Mr. Gengren HAO for their assistance in performing amplitude sweep tests in the laboratory.

Funding Open access funding provided by The Hong Kong Polytechnic University.

Data availability Some or all experimental data generated or used during this study are available from the corresponding author by request.

References

Adam L, Batzle M, Lewallen KT, Van Wijk K (2009) Seismic wave attenuation in carbonates. J Geophys Res Solid Earth. https://doi.org/10.1029/2008JB005890

Aksu I, Bazilevskaya E, Karpyn ZT (2015) Swelling of clay minerals in unconsolidated porous media and its impact on permeability. GeoResJ. https://doi.org/10.1016/j.grj.2015.02.003

Anderson RL, Ratcliffe I, Greenwell HC, Williams PA, Cliffe S, Coveney PV (2010) Clay swelling—a challenge in the oilfield. Earth Sci Rev 98(3–4):201–216. https://doi.org/10.1016/J.EARSCIREV.2009.11.003

ASTM Committee D-18 on Soil and Rock. (2008) Standard test method for laboratory determination of pulse velocities and ultrasonic elastic constants of rock. ASTM International

Atkinson BK (1984) Subcritical crack growth in geological materials. J Geophys Res. https://doi.org/10.1029/jb089ib06p04077

Auld BA, Green RE (1974) Acoustic fields and waves in solids: two volumes. Phys Today. https://doi.org/10.1063/1.3128926

Ba J, Zhao J, Carcione JM, Huang X (2016) Compressional wave dispersion due to rock matrix stiffening by clay squirt flow. Geophys Res Lett. https://doi.org/10.1002/2016GL069312

Bourbie T, Zinszner B (1985) Hydraulic and acoustic properties as a function of porosity in Fontainebleau Sandstone. J Geophys Res. https://doi.org/10.1029/jb090ib13p11524

Cadoret T, Marion D, Zinszner B (1995) Influence of frequency and fluid distribution on elastic wave velocities in partially saturated limestones. J Geophys Res. https://doi.org/10.1029/95JB00757

Carcione JM, Helle HB, Pham NH (2003) White's model for wave propagation in partially saturated rocks: comparison with poroelastic numerical experiments. Geophysics. https://doi.org/10.1190/1.1598132

Carpenter BM, Marone C, Saffer DM (2011) Weakness of the San Andreas Fault revealed by samples from the active fault zone. Nat Geosci. https://doi.org/10.1038/ngeo1089

Cha M, Cho GC, Santamarina JC (2009) Long-wavelength P-wave and S-wave propagation in jointed rock masses. Geophysics. https://doi.org/10.1190/1.3196240

Cho GC, Santamarina JC (2001) Unsaturated particulate materials—particle-level studies. J Geotech Geoenviron Eng. https://doi.org/10.1061/(asce)1090-0241(2001)127:1(84)

Crawford BR, Faulkner DR, Rutter EH (2008) Strength, porosity, and permeability development during hydrostatic and shear loading of synthetic quartz-clay fault gouge. J Geophys Res Solid Earth. https://doi.org/10.1029/2006JB004634

David EC, Fortin J, Schubnel A, Guéguen Y, Zimmerman RW (2013) Laboratory measurements of low-and high-frequency elastic moduli in Fontainebleau sandstone. Geophysics 78(5):D369–D379. https://doi.org/10.1190/geo2013-0070.1

Denneman AI, Drijkoningen GG, Smeulders DM, Wapenaar K (2002) Reflection and transmission of waves at a fluid/porous-medium interface. Geophysics 67(1):282–291. https://doi.org/10.1190/1.1451800

Fratta D, Santamarina JC (2002) Shear wave propagation in jointed rock: state of stress. Geotechnique. https://doi.org/10.1680/geot.2002.52.7.495

Hobiger M, Wegler U, Shiomi K, Nakahara H (2012) Coseismic and postseismic elastic wave velocity variations caused by the 2008 Iwate-Miyagi Nairiku earthquake, Japan. J Geophys Res Solid Earth. https://doi.org/10.1029/2012JB009402

Ikari MJ, Saffer DM, Marone C (2009) Frictional and hydrologic properties of clay-rich fault gouge. J Geophys Res Solid Earth. https://doi.org/10.1029/2008JB006089

Indraratna B, Premadasa W, Brown ET, Gens A, Heitor A (2014) Shear strength of rock joints influenced by compacted infill. Int J Rock Mech Min Sci. https://doi.org/10.1016/j.ijrmms.2014.04.019

Jeppson TN, Tobin HJ (2015) San Andreas fault zone velocity structure at SAFOD at core, log, and seismic scales. J Geophys Res Solid Earth. https://doi.org/10.1002/2015JB012043

Johnston DH, Toksoz MN, Timur A (1979) Attenuation of seismic waves in dry and saturated rocks—2. Mechanisms. Geophysics. https://doi.org/10.1190/1.1440970

Kaproth BM, Marone C (2014) Evolution of elastic wave speed during shear-induced damage and healing within laboratory fault zones. J Geophys Res Solid Earth. https://doi.org/10.1002/2014JB011051

Kenigsberg AR, Rivière J, Marone C, Saffer DM (2019) The effects of shear strain, fabric, and porosity evolution on elastic and mechanical properties of clay-rich fault gouge. J Geophys Res Solid Earth. https://doi.org/10.1029/2019JB017944

Kenigsberg AR, Rivière J, Marone C, Saffer DM (2020) Evolution of elastic and mechanical properties during fault shear: the roles of clay content, fabric development, and porosity. J Geophys Res Solid Earth. https://doi.org/10.1029/2019JB018612

Khazanehdari J, Sothcott J (2003) Variation in dynamic elastic shear modulus of sandstone upon fluid saturation and substitution. Geophysics. https://doi.org/10.1190/1.1567213

Knuth MW, Tobin HJ, Marone C (2013) Evolution of ultrasonic velocity and dynamic elastic moduli with shear strain in granular layers. Granul Matter. https://doi.org/10.1007/s10035-013-0420-1

Leurer KC (1997) Attenuation in fine-grained marine sediments: extension of the Biot-Stoll model by the "effective grain model" (EGM). Geophysics. https://doi.org/10.1190/1.1444250

Li JC, Ma GW (2009) Experimental study of stress wave propagation across a filled rock joint. Int J Rock Mech Min Sci. https://doi.org/10.1016/j.ijrmms.2008.11.006

Li D, Wei J, Di B, Ding P, Huang S, Shuai D (2018) Experimental study and theoretical interpretation of saturation effect on ultrasonic velocity in tight sandstones under different pressure conditions. Geophys J Int. https://doi.org/10.1093/gji/ggx536

Li D, Wei J, Di B, Shuai D, Tian L, Ding P (2020) Effect of fluid saturation on the shear modulus of artificial clay-rich tight sandstones. Geophys J Int. https://doi.org/10.1093/gji/ggaa124

Lucet N, Zinszner B (1992) Effects of heterogeneities and anisotropy on sonic and ultrasonic attenuation in rocks. Geophysics. https://doi.org/10.1190/1.1443313

Mavko G, Jizba D (1991) Estimating grain-scale fluid effects on velocity dispersion in rocks. Geophysics 56(12):1940–1949. https://doi.org/10.1190/1.1443005

Mavko G, Jizba D (1994) The relation between seismic P- and S-wave velocity dispersion in saturated rocks. Geophysics. https://doi.org/10.1190/1.1443537

Mezger TG (2006) The rheology handbook—for users of rotational and oscillatory rheometers. Appl Rheol 12:232

Mitchell JK, Soga K (2005) Fundamentals of soil behavior (Third Edition). New York: John Wiley & Sons.

Molyneux JB, Schmitt DR (2000) Compressional-wave velocities in attenuating media: a laboratory physical model study. Geophysics. https://doi.org/10.1190/1.1444809

Moyano B, Spikes KT, Johansen TA, Mondol NH (2012) Modeling compaction effects on the elastic properties of clay-water composites. Geophysics. https://doi.org/10.1190/geo2011-0426.1

Müller TM, Gurevich B, Lebedev M (2010). Seismic wave attenuation and dispersion resulting from wave-induced flow in porous rocks—A review. Geophysics 75(5):75A147-64. https://doi.org/10.1190/1.3463417

Niu F, Silver PG, Daley TM, Cheng X, Majer EL (2008) Preseismic velocity changes observed from active source monitoring at the Parkfield SAFOD drill site. Nature. https://doi.org/10.1038/nature07111

Pham NH, Carcione JM, Helle HB, Ursin B (2002) Wave velocities and attenuation of shaley sandstones as a function of pore pressure and partial saturation. Geophys Prospect. https://doi.org/10.1046/j.1365-2478.2002.00343.x

Pimienta L, Fortin J, Borgomano JV, Guéguen Y (2016) Dispersions and attenuations in a fully saturated sandstone: experimental evidence for fluid flows at different scales. Lead Edge 35(6):495–501. https://doi.org/10.1190/tle35060495.1

Pride SR, Berryman JG, Harris JM (2004). Seismic attenuation due to wave-induced flow. J Geophys Res Solid Earth 109(B1). https://doi.org/10.1029/2003JB002639

Pyrak-Nolte LJ, Myer LR, Cook NGW (1990) Anisotropy in seismic velocities and amplitudes from multiple parallel fractures. J Geophys Res. https://doi.org/10.1029/jb095ib07p11345

Suarez-Rivera FR, Myer LR, Cook NGW (1992) Study on the transmission of shear waves across thin liquid films and thin clay layers. The 33rd US Rock Mechanics/Geomechanics Symposium, Santa Fe, New Mexico, US. https://doi.org/10.1016/0148-9062(93)92424-o

Toksoz MN, Johnston DH, Timur A (1979) Attenuation of seismic waves in dry and saturated rocks—1. Laboratory measurements. Geophysics. https://doi.org/10.1190/1.1440969

Tuncay K, Yavuz Corapcioglu M (1996) Body waves in poroelastic media saturated by two immiscible fluids. J Geophys Res Solid Earth 101(B11):25149–25159. https://doi.org/10.1029/96JB02297

Viggiani G, Atkinson JH (1995) Interpretation of bender element tests. Geotechnique. https://doi.org/10.1680/geot.1995.45.1.149

Wang R, Hu Z, Wang Q (2021) A time-domain recursive method of SH-wave propagation through the filled fracture with linear viscoelastic deformation behavior. Waves Random Complex Media. https://doi.org/10.1080/17455030.2019.1643052

Wealthall GP, Steele A, Bloomfield JP, Moss RH, Lerner DN (2001) Sediment filled fractures in the Permo-Triassic sandstones of the Cheshire Basin: observations and implications for pollutant transport. J Contam Hydrol. https://doi.org/10.1016/S0169-7722(01)00104-8

Winkler KW, Nur A (1982) Seismic attenuation: effects of pore fluids and frictional-sliding. Geophysics 47(1):1–15. https://doi.org/10.1190/1.1441276

Wu W, Zhao J (2015) Effect of water content on P-wave attenuation across a rock fracture filled with granular materials. Rock Mech Rock Eng 48(2):7. https://doi.org/10.1007/s00603-014-0606-9

Yang H (2021) Fluid effects on the interaction of waves with rock joints. The Hong Kong Polytechnic University, Hong Kong

Yang H, Duan H, Zhu J (2020) Effects of filling fluid type and composition and joint orientation on acoustic wave propagation across individual fluid-filled rock joints. Int J Rock Mech Min Sci. https://doi.org/10.1016/j.ijrmms.2020.104248

Yang H, Duan HF, Zhu JB (2021) Thermal effect on compressional wave propagation across fluid-filled rock joints. Rock Mech Rock Eng 54(1):7. https://doi.org/10.1007/s00603-020-02254-5

Yang H, Duan HF, Zhu J (2023) Experimental study on the role of clay mineral and water saturation in ultrasonic P-wave behaviours across individual filled rock joints. Int J Rock Mech Min Sci. https://doi.org/10.1016/j.ijrmms.2023.105393

Zhu JB, Perino A, Zhao GF, Barla G, Li JC, Ma GW, Zhao J (2011) Seismic response of a single and a set of filled joints of viscoelastic deformational behaviour. Geophys J Int 186(3):7. https://doi.org/10.1111/j.1365-246X.2011.05110.x